Eur. Phys. J. B **43**, 453–461 (2005)
DOI: 10.1140/epjb/e2005-00078-6

THE EUROPEAN PHYSICAL JOURNAL B

Phonon vibrational frequencies and elastic properties of solid SrFCl. An ab initio study

P. Labéguerie[1], F. Pascale[2], M. Mérawa[3,a], C. Zicovich-Wilson[4], N. Makhouki[3], and R. Dovesi[5]

[1] Laboratoire de Chimie Théorique et de Physico-Chimie Moléculaire, UMR 5624, FR 'IPREM' 2606, IFR, rue Jules Ferry 64075 Pau Cedex, France
[2] Laboratoire de Cristallographie et Modélisation des Matériaux Minéraux et Biologiques (LCM3B) UMR 7036 - CNRS, Université Henri Poincaré, Nancy I BP 239, Boulevard des Aiguillettes, 54506 Vandoeuvre-les-Nancy Cedex, France
[3] Laboratoire de Chimie Théorique et de Physico-Chimie Moléculaire, UMR 5624, FR 'IPREM' 2606, IFR, rue Jules Ferry 64000 Pau, France
[4] Facultad de Ciencias, Universidad Autónoma del Estado de Morelos, Av. Universidad 1001, Col. Chamilpa, 62210 Cuernavaca (Morelos), Mexico
[5] Dip. Chimica IFM, University of Torino, Via Giuria 7, 10125 Torino, Italy

Received 21 September 2004 / Received in final form 17 December 2004
Published online 30 March 2005 –

Abstract. The phonon vibrational frequencies, electronic and elastic properties of SrFCl, one of the members of the alkaline-earth fluorohalide family crystallizing with the PbFCl-type structure, have been investigated, for the first time, at the ab initio level, by using the periodic CRYSTAL program. Both Hartree-Fock (HF) and density functional theory (DFT) Hamiltonians have been used, with the latter in its local density, gradient-corrected (PW91), and hybrid (B3LYP) versions. The structural and elastic properties are in good agreement with experiment, with the exception of those calculated within the local density approximation, which were found to be systematically under-estimated (distances) or over-estimated (elastic properties). As regards the phonon frequencies, B3LYP and PW91 provide excellent results, the mean absolute difference with respect to the experimental Raman data being 4.1% and 3.6%, respectively.

PACS. 78.30.-j Infrared and Raman spectra – 71.15.Mb Density functional theory, local density approximation, gradient and other corrections – 62.20.Dc Elasticity, elastic constants

1 Introduction

During the last decade, a number of theoretical and experimental papers were devoted to the study of the structural, optical and physical properties of alkaline-earth fluorohalides MFX(M = Ba, Ca, Sr; X = Cl, Br, I) [1–20]. Alkaline-earth fluorohalides are layered compounds crystallizing in the tetragonal PbFCl-type structure (matlockite-type structure). These layered materials have a more or less two-dimensional character, with relatively weak bonding between the two adjacent Cl^- layers. Fluorohalides present therefore interesting behaviour such as changing properties during pressure-driven phase transitions.

The crystal structure at room and high pressure, high-temperature X-ray diffraction, phase transition as a function of temperature and pressure, Raman and infrared active phonons frequencies, and elastic properties of theses compounds have been simulated previously by using molecular dynamics [2,11,12,15–18], and tight-binding muffin-tin type schemes [13,14].

In this work, the electronic, structural, elastic and vibrational properties of SrFCl, a member of the matlockite family, are investigated with the periodic ab initio program CRYSTAL03 [21] that uses a localized basis set. In spite of their technologically attractive properties (e.g. for X-ray image storage [22–25]), to our knowledge, no ab initio calculation of phonon vibrational frequencies or elastic constants of SrFCl has been reported so far.

The role of electron correlation is investigated at the Density Functional Theory (DFT) level, by using different treatments of the exchange-correlation potential, ranging from the local density [26] and gradient [27–30] corrected variants, to hybrid B3LYP [31,32] scheme, where part of the "exact" Hartree-Fock exchange is used. To complete the landscape of possibilities, Hartree-Fock calculations were also performed. Therefore, we should be able to gain some perspective on the performance of various Hamiltonians in predicting the structural, elastic and vibrational properties of fluorohalides.

The paper is organised as follows: Section 2 provides the methodological tools and a description of the computational aspects. The numerical results, which include

[a] e-mail: mohammadou.merawa@univ-pau.fr

structural parameters, electronic structures, energies, elastic constants and phonons vibrational frequencies are discussed and compared with experimental data in Section 3. Unless stated otherwise, atomic units are used throughout this paper.

2 Method and computational details

Calculations were performed with a development version of the periodic ab initio CRYSTAL03 program [21]. Crystalline Orbitals are represented as linear combinations of Bloch Functions (BF), and are evaluated over a regular three-dimensional mesh in reciprocal space. Each BF is built from local Atomic Orbitals (AO), which are contractions (linear combinations with constant coefficients) of Gaussian-Type Functions (GTF), each GTF being the product of a Gaussian times a real solid spherical harmonic. All electron basis sets have been used for Cl and F atoms [33,34]. They consist of 8-6311(1) and 7-311(1) contractions for Cl and F, respectively, where the first figure refers to an *s* shell, the others to *sp* shells; *d* shell contractions are given in parentheses. There are then 22 and 18 AOs for Cl and F, respectively. The exponents of the outer *sp* and *d* shells have been re-optimized at the HF level (and used as such for the other Hamiltonians) to the following values (in bohr^{-2} units): α(Cl, *sp*) = $\{0.415, 0.200\}$, α(Cl, *d*) = 0.355; α(F, *sp*) = $\{0.440, 0.158\}$, α(F, *d*) = 0.786. A Hay-Wadt [35–37] effective core potential (ECP) has been adopted for strontium; 2111(21) contractions of GTFs have been used for the valence electrons (the optimized exponents are: α(Sr, *sp*) = $\{0.736, 0.330, 0.17\}$; α(Sr, *d*) = 0.363). Standard values for the computational tolerances as defined in the CRYSTAL03 manual [21] have been adopted for all steps of the calculation, except for the vibrational frequencies, that require more severe conditions.

In the geometry optimization, a structural relaxation procedure consisting of two independent steps was iteratively performed. In the first step, the cell parameters (a, c) were optimized with the atoms at fixed fractional positions. Cell optimization was carried out by means of a modified Polak-Ribiere algorithm, in which the energy gradients were evaluated numerically by means of the central-difference formula [38]. In the second step, atomic positions $(x, y, z$, fractional coordinates) were fully relaxed at fixed cell parameters. Forces on atoms were obtained by using the analytical HF [39,40] and DFT [41] energy gradients and were used to relax the atoms to equilibrium by using a modified conjugate gradient algorithm proposed by Schlegel [42]. Convergence was tested on the RMS and the absolute value of the largest component of the gradients and the estimated displacements. The threshold for the maximum force, the RMS force, the maximum atomic displacement, and the RMS atomic displacement on all atoms have been set to 0.00045, 0.00030, 0.00180 and 0.00120 a.u., respectively. The atomic position optimization was considered complete when these four conditions were satisfied. The crystal symmetry was maintained during the optimization process. The two-step structure optimization process was repeated until both the cell parameters and the atomic positions convergence criteria were satisfied [43].

Three functional forms have been chosen from the large variety of local and non-local exchange-correlation potentials available. They are as follows:

- LV: local [26] exchange plus Vosko-Wilk-Nusair [44] correlation potential;
- PW91: Perdew-Wang [27–30] exchange and correlation potential.
- B3LYP: Becke's three-parameter exchange functional [31] and the non-local Lee-Yang-Parr correlation functional [32].
- HF: Hartree-Fock.

The results have thus been obtained with four different Hamiltonians, giving some insight into the differences one can expect when changing this important parameter of the calculation.

A Taylor expansion of the unit cell energy to second order as a function of the strain,

$$E(\varepsilon) = E(0) + \sum_{i=1}^{6} \left[\frac{\partial E}{\partial \varepsilon_i}\right]_0 \varepsilon_i + \frac{1}{2} \sum_{i,j=1}^{6} \left[\frac{\partial^2 E}{\partial \varepsilon_i \varepsilon_j}\right]_0 \varepsilon_i \varepsilon_j$$

has been considered for the calculation of the elastic constants. $E(0)$ stands for the energy of the equilibrium configuration, ε_i refers to the strain components expressed according to Voigt's notation with a single index $(i = 1, 6)$. The elastic constants C_{ij}, are related to the second derivatives of the energy with respect to strain components as follows:

$$C_{ij} = \frac{1}{V} \left[\frac{\partial^2 E}{\partial \varepsilon_i \partial \varepsilon_j}\right]_0 .$$

Energy second derivatives were evaluated numerically. Since SrFCl is a tetragonal crystal with a D_{4h}^7 space group, there are six non-vanishing independent components of the elastic tensor, namely C_{11}, C_{12}, C_{13}, C_{33}, C_{44} and C_{66}. Fifteen ε_i values in the interval $[-0.020, +0.020]$ Å interval were considered for the fitting. During the deformation of the unit cell with a given strain, symmetry may be reduced and additional degrees of freedom appear that must be fully relaxed.

For this tetragonal system, the linear compressibilities parallel ($\parallel$) and perpendicular ($\perp$) to the C_4 axis are related to the elastic constants in the following way:

$$\chi_{\parallel} = \frac{C_{11} + C_{12} - 2C_{13}}{[C_{33}\,(C_{11} + C_{12}) - 2C_{13}^2]}$$
$$\chi_{\perp} = \frac{C_{33} - C_{13}}{[C_{33}\,(C_{11} + C_{12}) - 2C_{13}^2]}.$$

The volume compressibility χ, given by: $\chi = \chi_{\parallel} + 2\chi_{\perp}$, can then be evaluated.

We refer to a recent paper [45] for a complete discussion of the computational conditions and other numerical aspects concerning the calculation of the phonon frequencies at the $\Gamma = (0, 0, 0)$ point. The mass-weighted Hessian

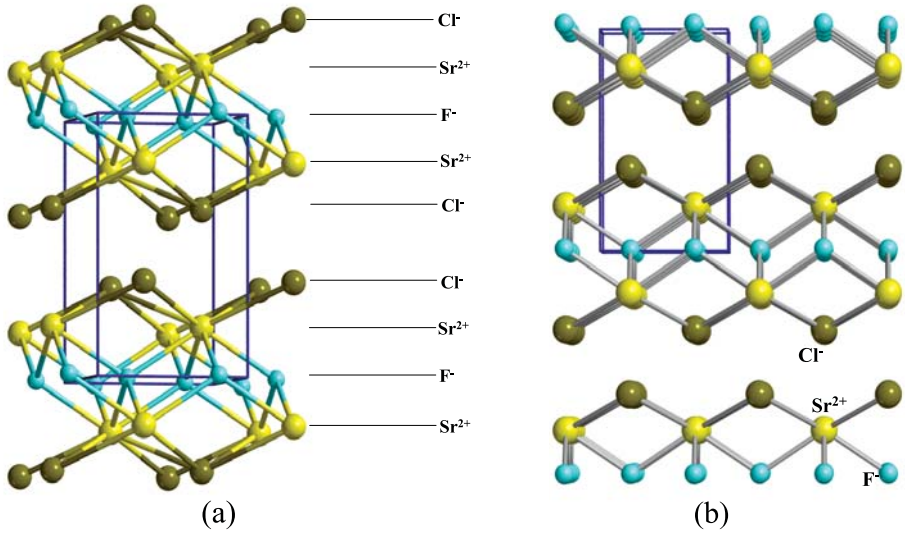

Fig. 1. B3LYP optimized structures of SrFCl (1a) and of the isolated two-dimensional layer (1b).

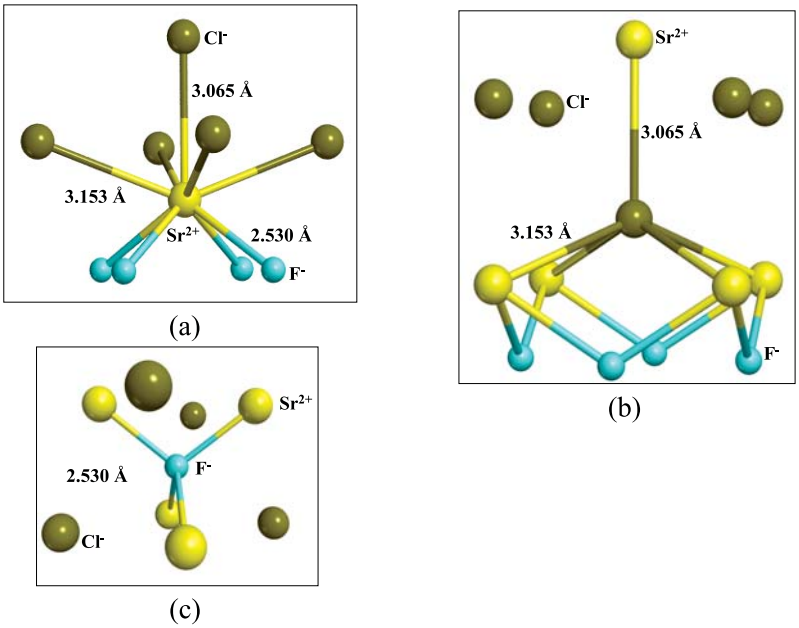

Fig. 2. Atomic coordination in SrFCl.

matrix is obtained by numerical differentiation of the analytical first derivatives, calculated at geometries obtained by incrementing in turn each of the 3N nuclear coordinates by a small amount u with respect to the equilibrium geometry. In the case of ionic compounds, long range Coulomb effects due to coherent displacement of the crystal nuclei are neglected in the above calculation, as a consequence of imposing the periodic boundary conditions [46]. The mass-weighted Hessian needs to be corrected in order to obtain the longitudinal optical (LO) modes [47]. The electronic dielectric and Born charge tensors have therefore been calculated with the four Hamiltonians.

As regards the grid for the numerical integration of the exchange-correlation term, 75 radial points (the default value is 55) and 974 (default 434) angular points in a Lebedev scheme have been used. The condition for the SCF convergence is set to 10^{-10} hartree. The shrinking factor of the reciprocal space net is set to 8, corresponding to 75 reciprocal space points at which the Hamiltonian matrix was diagonalized. The total energies obtained with this mesh is fully converged.

3 Results and discussion

The tetragonal structure of SrFCl is illustrated in Figure 1a. The unit cell has two molecular units with planes of identical ions in the sequence $F^- - Sr^{2+} - Cl^- - Cl^- - Sr^{2+} - F^-$ perpendicular to the c-axis as depicted in Figure 1b. All atoms are in special positions. Strontium is nine-fold coordinated by 4 F ions at 2.530 Å (B3LYP results), one Cl at 3.065 Å, and four Cl at 3.153 Å (see Fig. 2). Cl ions are connected to 5 Sr atoms in a square pyramidal configuration, whereas the F ions are surrounded by 4 Sr ions. The layered structure of the compound is confirmed by the large distance between two adjacent Cl planes (3.564 Å).

Table 1. Calculated and experimental equilibrium lattice parameters and interatomic distances (in Å). Percentage deviation with respect to experiment are given in parentheses.

SrFCl	HF	B3LYP	PW91	LV	Exp. Ref. [20]
a	4.208 (+1.9)	4.188 (+1.5)	4.149 (+0.6)	4.032 (−2.3)	4.126
c	7.140 (+2.5)	6.988 (+0.4)	6.960 (+0.02)	6.728 (−3.3)	6.958
z_{Sr}	0.1989	0.2033	0.2066	0.2071	0.2015
z_{Cl}	0.6438	0.6419	0.6435	0.6468	0.6489
Sr-F	2.538 (+1.7)	2.530 (+1.4)	2.524 (+1.2)	2.451 (−1.7)	2.494
Sr-Cl	3.176 (+2.5)	3.065 (+1.5)	3.041 (−1.8)	2.951 (−4.7)	3.098
F-F	2.975 (+1.9)	2.961 (+2.0)	2.934 (+0.5)	2.851 (−2.3)	2.918
F-Cl	3.300 (+3.0)	3.263 (+2.0)	3.234 (+1.1)	3.122 (−2.4)	3.198
Cl-Cl	3.615 (+1.0)	3.564 (-0.5)	3.549 (+0.8)	3.461 (−3.3)	3.579

Table 2. Total energy of the atoms and compounds at equilibrium (per formula unit, in hartree). IE (eV) interlayer energy, evaluated as the difference between the bulk energy and the energy of an isolated two-dimensional layer, after correction for the BSSE. Formation energy ΔE_f (eV) of SrFCl, SrF_2 and $SrCl_2$ from the isolated atoms, and reaction energy ΔE_r (eV) evaluated according to the reaction $SrF_2 + SrCl_2 \rightarrow 2SrFCl$.

	HF	B3LYP	PW91	LV	Exp. Ref. [50]
Sr	−30.09619	−30.39468	−30.42737	−30.31230	
F	−99.37401	−99.70167	−99.70065	−99.07088	
Cl	−459.44914	−460.08415	−460.11631	−458.63305	
SrF_2	−229.31415	−230.36454	−230.41650	−229.11545	
$SrCl_2$	−949.38241	−950.98591	−951.10444	−948.08246	
SrFCl	−589.35367	−590.68119	−590.76757	−588.61119	
SrFCl (Slab)	−589.34322	−590.66880	−590.75422	−588.59320	
ΔE_f(SrFCl)	11.818	13.624	14.237	16.189	
ΔE_f($SrCl_2$)	10.556	11.508	12.093	13.715	12.611
ΔE_f(SrF_2)	12.787	15.415	15.995	17.986	15.891
ΔE_r	0.293	0.324	0.386	0.666	
IE	0.284	0.337	0.363	0.489	

The optimized geometrical data obtained with the four Hamiltonians are listed in Table 1 together with the experimental findings [48]. B3LYP and PW91 provide quite accurate geometries (the latter more than the former), whereas HF tends to overestimate distances, and LV underestimate them even more.

Table 2 lists the energy data relevant to the calculation of the SrFCl formation energies ($\Delta \mathrm{E}_f$) and the energy of the reaction, experimentally used to grow the SrFCl crystal:

$$SrF_2 + SrCl_2 \rightleftharpoons 2SrFCl.$$

In a recent paper it has been shown [49] that the correction that brings the experimental room temperature (RT) formation energy down to the static limit, where it can be compared to the calculated values, is very small, and can be neglected in most cases. Therefore, the calculated binding energies are directly compared to the experimental RT data in Table 2. The formation energy ΔE_f of SrF_2 and $SrCl_2$, computed at B3LYP and PW91 level, are in very good agreement with experiment [50], deviations being within 3%. As expected, HF underestimates the experimental ΔE_f by some 16−19%, for $SrCl_2$ and SrF_2, respectively. At the other extreme, LV provides ΔE_f data that are higher than experiment by about 10%. The calculated formation energies of SrFCl, is intermediate between those obtained for $SrCl_2$ and SrF_2. Unfortunately, we have not been able to find any experimental formation energy of this compound. There is, indeed, a close correlation between the binding energy of SrFCl and those of $SrCl_2$ and SrF_2. This suggests that the experimental value should lie between the values measured for $SrCl_2$ and SrF_2, and be very close to the calculated B3LYP and PW91 formation energies.

The interlayer energies, IE, calculated as the difference between the bulk energy and the energy of an isolated two-dimensional layer, whose fractional coordinates have been re-optimized, are listed in Table 2. The small values (the Basis-Set-Superposition Error (BSSE) has been taken into account) indicate that the inter-layer interaction (IE) is weak, although not so weak as in other cases like in brucite [51], that has been calculated to be only 10% of the present values. SrFCl can then be seen as a two-dimensional system, with relatively weak interlayer interaction.

The Mulliken net atomic charges (q) and bond populations (b) are collected in Table 3. The Sr, F and

Table 3. Mulliken net atomic charges (q) and bond populations for SrFCl computed with different Hamiltonians. Data in $|e|$.

	HF	B3LYP	PW91	LV
q(Sr)	+1.808	+1.716	+1.676	+1.637
q(F)	−0.978	−0.949	−0.934	−0.925
q(Cl)	−0.830	−0.766	−0.742	−0.712
b(Sr-F)	−0.024	−0.022	−0.020	−0.039
b(Sr-Cl)	+0.017	+0.021	+0.023	+0.022
b(F-Cl)	+0.001	+0.002	+0.002	−0.002

Table 4. Elastic constants C_{ij} (GPa) of SrFCl for each Hamiltonian. Percentage deviation with respect to the experimental selected values given in references [5,6] enclosed in parentheses.

	HF	B3LYP	PW91	LV	Exp Ref. [5,6]
c_{11}	96.5 (+5.5)	92.7 (+1.6)	95.2 (+4.2)	118.0 (+22.7)	91.2 ± 0.2
c_{33}	76.1 (−1.0)	79.9 (+3.8)	83.9 (+8.3)	112.7 (+31.8)	76.9 ± 0.3
c_{44}	30.4 (+5.6)	27.9 (−2.8)	29.7 (+3.4)	40.9 (+29.8)	28.7 ± 0.2
c_{66}	33.5 (+6.0)	30.2 (−4.1)	31.9 (+1.6)	35.4 (+11.0)	31.5 ± 0.2
c_{12}	29.5 (+0.7)	32.3 (+9.3)	31.5 (+7.0)	47.2 (+37.9)	29.3 ± 2.2
c_{13}	43.0 (+3.3)	45.2 (+8.0)	43.8 (+5.0)	56.2 (+26.0)	41.6 ± 1.4

Table 5. Linear compressibilities parallel ($\chi_\parallel \times 10^3$ GPa^{-1}) and perpendicular ($\chi_\perp \times 10^3$ GPa^{-1}) to the C_4 axis, volume compressibilities ($\chi \times 10^3$ GPa^{-1}) and the corresponding bulk and linear moduli (B_0, $B_\parallel$ and $B_\perp$, in GPa).

	HF	B3LYP	PW91	LV	Exp Ref. [5,6]
$\chi_\parallel$	4.9	4.1	4.1	3.0	4.6
$\chi_\perp$	4.1	4.1	4.3	3.2	4.3
χ	13.1	12.3	12.6	9.4	13.2
$(\frac{\chi_\perp}{\chi_\parallel})$	0.84	1.00	1.03	1.07	0.93
B_0	76.3	81.3	79.1	106.4	75.8
$B_\parallel$	204.1	243.9	241.5	333.3	217.4
$B_\perp$	243.9	243.9	235.3	312.5	232.6

Table 6. Effective dynamical charges along ($e^*_\parallel$) and perpendicular ($e^*_\perp$) to the C_4-axis for each ion, and dielectric constant components, calculated with the four Hamiltonians.

		HF	B3LYP	PW91	LV
Sr	$e^*_\perp$	2.390	2.509	2.525	2.531
	$e^*_\parallel$	2.414	2.525	2.541	2.547
F	$e^*_\perp$	−1.193	−1.247	−1.251	−1.282
	$e^*_\parallel$	−1.302	−1.369	−1.398	−1.448
Cl	$e^*_\perp$	−1.209	−1.256	−1.274	−1.249
	$e^*_\parallel$	−1.117	−1.153	−1.142	−1.099
	$\varepsilon_\infty(xx)$	2.059	2.387	2.571	2.792
	$\varepsilon_\infty(zz)$	2.048	2.385	2.568	2.777

Cl Mulliken charges are very close to their formal values, confirming that the compound is very ionic. As expected, HF provides a more ionic picture than B3LYP and PW91, whereas the LV net charges are the smallest. Bond populations are extremely small (again confirming the ionic picture) in all cases.

The elastic constants are reported in Table 4, together with the experimental data [6]. Percentage deviation with respect to the selected experimental values given in reference [6] are also given. Since LV describes SrFCl as more compact and rigid than it really is (this is a usual feature for this functional), the quality of the LV results is expected to be poorer than that from the other functionals. This is confirmed by the data in the table, showing that B3LYP and PW91 and also HF perform quite well: the percentage error with respect to experiment is below 6%, with only three exceptions (C_{33} and C_{12} at the PW91 level and C_{12} at B3LYP level).

The linear compressibilities along the directions parallel ($\chi_\parallel$) and perpendicular ($\chi_\perp$) to the C_4 axis, the volume compressibilities (χ) as well as the bulk ($B_0 = 1/\chi$) and linear moduli ($B_\parallel = 1/\chi_\parallel$, $B_\perp = 1/\chi_\perp$) deduced from the calculated elastic constants with the four Hamiltonians are listed in Table 5, together with the experimental data. As expected, all but LV computed values are quite close to experiment. The $\chi_\perp/\chi_\parallel$ ratio show that the linear compressibility is nearly isotropic.

The dielectric constant and effective dynamical charge components, used for the calculation of the LO-TO splitting, are given in Table 6. Tensors are diagonal, with $e^*_{xx} = e^*_{yy} = e^*_\perp$; the $e^*_\parallel$ and $e^*_\perp$ components are very similar, so that the tensor is nearly isotropic. This is even more true for the dielectric tensor, where differences are always smaller than 0.01. The Born charges are larger than the formal charges (+2 and $-1|e|$), indicating a relatively high polarisability of the ions. As usual, HF and LV are at the two extremes, but the differences for the e^* tensor are in all cases under 10%, except for $e^*_\parallel$ for the fluorine atom. In the case of chlorine the LDA $e^*_\parallel$ is lower than the value calculated at the HF level. The dielectric constant components, on the contrary, differ between HF and LDA

Table 7. Calculated and experimental Raman [52] and Infrared [53] active modes in cm^{-1}. Percentage deviation with respect to experimental data are enclosed in parentheses.

		HF	B3LYP	PW91	LV	Exp Ref. [52]	Exp Ref. [53]
Raman	A_{1g}	163 (+4.9)	167 (+7.2)	170 (+8.8)	188 (+17.6)	155	
		218 (+10.1)	206 (+4.9)	204 (+3.9)	219 (+10.5)	196	
	B_{1g}	271 (+10.3)	231 (−4.9)	230 (−5.3)	257 (+5.8)	243	
	E_g	122 (+12.3)	100 (−6.5)	107 (0)	114 (+6.5)	107	
		183 (+8.7)	167 (0)	168 (+0.6)	194 (+13.9)	167	
		325 (+8.3)	294 (−1.3)	289 (−3.0)	312 (+4.5)	298	
Infrared	A_{2u} (TO)	147 (−19.2)	146 (−19.8)	158 (−13.2)	185 (+1.6)		182
		347 (+2.0)	314 (−7.6)	309 (−9.1)	332 (+2.4)		340
	A_{2u} (LO)	229	228	229	243		
		402	372	370	395		
	E_u (TO)	137 (−4.2)	117 (−18.0)	131 (−8.4)	162 (+11.7)		143
		254 (−0.4)	204 (−20.0)	221 (−13.3)	249 (−2.4)		255
	E_u (LO)	174	153	161	186		
		349	314	323	346		

Table 8. Effect of isotopic substitution on B3LYP harmonic frequencies of bulk SrFCl. $\Delta\omega$ stands for the deviations of harmonic frequencies of the isotopically substituted bulk with respect to the non-substituted system; the NORM column reports the numbers in the $\Delta\omega$ column multiplied by a normalising factor such that the largest shift is equal to 10 cm^{-1} for each isotopical substitution. The harmonic frequency shifts going from bulk to a single layer are also reported in the last column. All data in cm^{-1}.

		BULK	^{84}Sr		^{37}Cl		^{22}F		(Slab)
MODE	Symmetry	ω	$\Delta\omega$	NORM	$\Delta\omega$	NORM	$\Delta\omega$	NORM	$\Delta\omega$
1	E_g	294	0.09	0.3	−0.08	0.2	−20.29	10.0	−2.29
1'	E_u	204	0.59	1.7	0.08	0.2	−12.35	6.1	−4.33
2	B_{1g}	231	0.00	0.0	0.00	0.0	−16.37	8.1	+3.83
2'	A_{2u}	314	0.27	0.8	−1.11	2.2	−18.27	9.0	+60.37
3	A_{1g}	206	0.46	1.3	−5.08	10.0	0.00	0.0	−16.72
3'	A_{2u}	146	+1.16	3.4	−2.50	4.9	−0.42	0.2	+29.66
4	E_g	167	0.06	0.2	−4.45	8.9	−0.18	0.1	−61.83
4'	E_u	117	+0.68	2.0	−2.38	4.7	−0.06	0.0	−11.23
5	A_{1g}	167	+3.46	10.0	−0.46	0.9	0.00	0.0	−52.43
6	E_g	100	+2.24	6.5	−0.05	0.1	−0.08	0.0	−15.33

by as much as 35%, (from 2.06 to 2.79 for $\varepsilon_\infty(xx)$, and from 2.05 to 2.78 for $\varepsilon_\infty(zz)$, with B3LYP and PW91 in between the two extremes, and B3LYP closest to HF).

We can now consider the phonon spectra at the Γ point. Group theory analysis applied to the P4/nmm group predicts a distribution of the 18 degrees of freedom (two SrFCl molecules in the unit cell) into modes belonging to the following irreducible representation [52–54],

$$\Gamma_{18} = 2A_{1g} + B_{1g} + 3E_g + 3A_{2u} + 3E_u$$

with six Raman active modes ($2A_{1g}, 1B_{1g}, 3E_g$), four IR active modes ($2A_{2u}$ and $2E_u$), and two acoustic modes (A_{2u} and E_u) yielding zero frequencies as the phonon wave vector $q \mapsto 0$.

In Table 7 the phonon vibrational frequencies, as well as the available experimental data [15,52] are given. The agreement between theoretical and experimental frequencies is remarkably good for the Raman mode. The mean absolute percentage difference is 3.6 and 4.1% at PW91 and B3LYP levels, respectively, whereas it rises to 9.1 and 9.8 for HF and LV.

Experimental IR data are not available for some of the modes. The percentage deviations with respect to the available experimental data [53] are larger than for the Raman active modes (see Tab. 7).

Modes have been analysed in terms of atomic displacements both graphically [55] and by using isotopic substitutions as a complementary tool. The mass-weighted Hessian matrix has been re-diagonalised by substituting subsequently ^{88}Sr (isotopic abundance of 83%) by ^{84}Sr (isotopic abundance of 1%); ^{35}Cl (isotopic abundance of 76%) by ^{37}Cl (isotopic abundance of 24%). ^{19}F has a 100% natural abundance; however, in order to identify the F contributions to the modes, we used a fictitious mass of ^{22}F. The B3LYP results are given in Table 8 and Figure 3. For clarity, frequency shifts in Table 8 have also

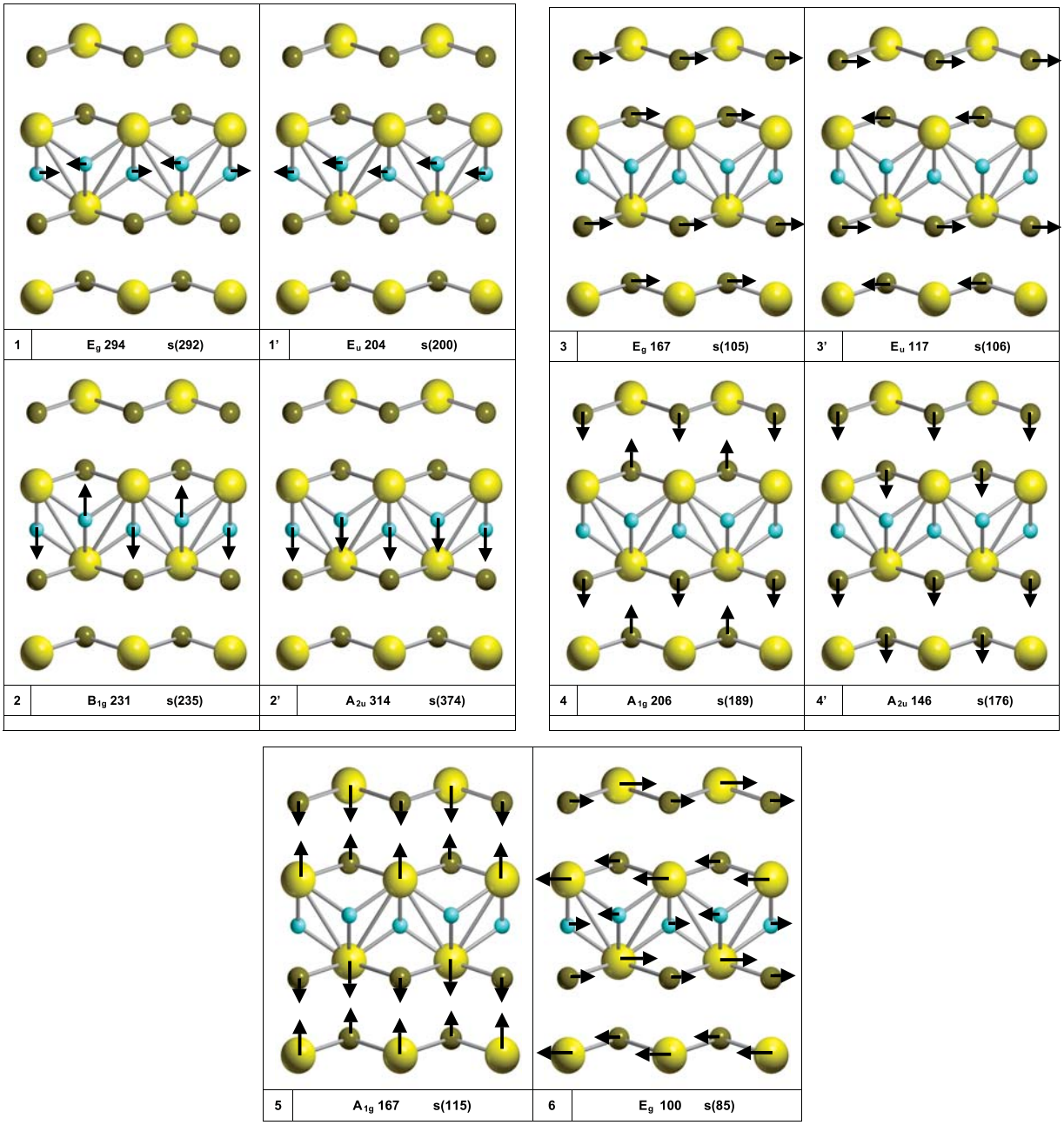

Fig. 3. Atomic displacements for all normal modes and frequencies. Arrows show the motions of atoms in a complete layer and parts of the adjacent layer. Frequencies for the single two-dimensional layer are indicated as s(value). All data in cm^{-1}.

been scaled in such a way that the largest shift for each isotopic substitution is equal to 10 cm^{-1} (see column NORM in Tab. 8). Because of the layered structure of SrFCl, we also performed the calculation of the vibrational spectra of a single two-dimensional layer containing two atomic units, whose energy is given in Table 2. The F column in Table 8 shows very clearly that the four modes with the highest frequency involve essentially the F atom, with a shift ranging from 12.4 to 20.3 cm^{-1}, whereas all the other modes shift by less than 0.5 cm^{-1}. These modes are labelled as 1, 1' and 2, 2' in Figure 3. The in-plane modes 1 and 1' (at 294 and 204 cm^{-1}) have the same frequency in the bulk and in the slab. The E_u mode is about 90 cm^{-1} lower than the E_g mode, because in the former, atoms in the same plane move in the same direction, reducing the electrostatic repulsion.

For the displacements along the C_4 axis, the B_{1g} mode at 231 cm^{-1} has lower frequency (about 83 cm^{-1}) than the A_{2u} mode, because it avoids the strong polarisation of the crystal that takes place in the latter; B_{1g} is about the same in the bulk and in the slab, whereas A_{2u} increases by about 60 cm^{-1} in the slab, due to the lack of compensating effects from the other layers.

Let us now consider the four frequencies involving mainly the Cl atoms. In Table 8, the Cl column shows that a shift ranging between 2.4 and 5.1 cm^{-1} is observed for the 3, 3', 4, 4' modes, whereas the largest shift of the other modes on ^{37}Cl substitution never exceeds 1.1 cm^{-1}. The two in-plane modes at 167 cm^{-1} and 117 cm^{-1} (3 and 3') parallel the behaviour of 1 and 1', the "u" versus "g" splitting being smaller in the former than latter (50 vs. 90 cm^{-1}). The E_g modes difference between the bulk and the slab is relatively large, because the Cl^- ions belonging to adjacent layers move in opposite directions, generating some $Cl^- - Cl^-$ repulsion (the frequency in the layer is lower). This interlayer effect is much smaller in E_u (only 11 cm^{-1}) because the Cl^- ions of adjacent layers move in phase. Also the splitting between the A_{1g} and A_{2u} modes (4 and 4') is smaller than for 2 and 2' (60 versus 83 cm^{-1}): due to the position of the Cl^- ions in the slab, the ungerade frequency is lower than the gerade one. The interlayer interaction is higher than for the F modes: it is about 17 cm^{-1} in A_{1g} (the slab frequency is lower) and 30 cm^{-1} in A_{2u}, where it increases in going from bulk to slab due to the lack of attraction from the Sr^{2+} on the Cl^- ions of the adjacent layers.

The last two modes, 5 and 6, at very low frequency, mainly involve the Sr atom (see Tab. 8), where a shift of 3.46 and 2.24 cm^{-1} is observed for these two modes, whereas the highest ^{84}Sr shift for all the other modes is just 1.16 cm^{-1}. The isotopic effect for Sr is quite small because the masses of the two isotopes differ by 5%, whereas in the Cl and F cases, they differ by 11% and 14%, respectively. These two modes, represented at the bottom of Figure 3, are essentially the relative motion of the two SrFCl units, in the (x, y) plane and in the z direction.

4 Conclusion

The electronic, structural, elastic and vibrational properties of SrFCl have been computed at the ab initio level with 4 different Hamiltonians. Good agreement with experiment has been obtained with B3LYP and PW91, whereas HF and LV provide in many cases results of lower quality.

A full analysis and classification of the vibrational modes has been performed. The results obtained show that B3LYP is generally good for almost any property of SrFCl. Similar performances were also observed for other materials [49,56,57]. However, in contrast with previous calculations [56] B3LYP and PW91 give results of the same quality. This suggests that correlation effects are very important and must be properly taken into account for an accurate description of systems like SrFCl where polarisation and charge transfer effects play a crucial role. New exchange-correlation functionals [58,59] have recently been tailored to provide a better description of such effects and one should then expect more accurate results. Unfortunately, they are not yet implemented in solid state ab initio codes but it will be interesting to evaluate their performance when available.

Mittal et al. [18] recently reported similar calculations on alkaline-earth fluorohalides by using a shell model with transferable interatomic potentials. Their results for the lattice parameters, elastic constants, bulk modulus, IR and Raman frequencies are in good agreement with experiment and close to the present B3LYP results. Shell model calculations are a cheaper alternative to ab initio methods, but they are based on a specific parametrization of the model potential making them less transferable to other systems. This limits their applicability to other systems, such as doped alkaline-earth fluorohalides, for which further parameters would be needed.

The results reported, available for the first time at the ab initio level, for structural, elastic, electronic and vibrational properties, show the feasibility and accuracy of ab initio methods in the study of heavy alkali-earth fluorohalides and will be a good starting point for future work on doped systems.

This work was supported in part by "Centre National de la Recherche Scientifique" (CNRS) and the "Ministère de l'Enseignement Supérieur et de la Recherche" (MESR). Some of the calculations were carried out on the IBM/SP3 computer at the "Centre Informatique National de l'Enseignement Supérieur" (CINES). We thank the scientific council of IDRIS for its support to this project.

References

1. B. Sundarakannan, T.R. Ravindran, R. Kesavamoorthy, S.V.M. Satyanarayana, Solid. State Comm. **124**, 385 (2002)
2. M. Liu, T. Kurobori, Y. Hirose, Phys. Stat. Sol. **225**, 20 (2001)
3. N. Subramanian, N.V. Chandra Shekar, P.Ch. Sahu, M. Yousuf, K. Govinda Rajan, Phys. Rev. B **58**, 555 (1998)
4. M. Pasero, N. Perchiazzi, Minera. Magazine **60**, 833 (1996)
5. M. Fischer, M. Sieskind, A. Polian, A. Lahmar, J. Phys. Condens. Matt. **5**, 2749 (1993)
6. M. Fischer, A. Polian, M. Sieskind, J. Phys.: Condens. Matt. **6**, 10407 (1994)
7. H.P. Beck, A. Limmer, W. Denner, H. Schulz, Acta Cryst. **39**, 401 (1983)
8. L.H. Brixner, J.D. Bierlein, V. Jhonson, in *Eu^{2+} Fluorescence and its Application in Medical X-Ray Intensifying Screens*, Current Topics in Material Science 4, edited by E. Kaldis (North Holand, Amsterdam, 1980)
9. G. Blasse, in *Solid State Luminescence -Theory, Materials and Devices*, edited by A.H. Kitai (Chapman and Hall, London, 1993), Chap. 11. p. 349, and references therein
10. A.R. Lakhshmanan, K. Govinda Rajan, Radiat. Prot. Dosim. **55**, 247 (1994)
11. T. Kurobori, S. Kozake, T. Kawamoto, Y. Hirose, Jpn J. Appl. Phys. **39**, 537 (2000)
12. T. Kurobori, M. Liu, H. Tsunekawa, Y. Hirose, M. Takeuchi, Radiation Effects and Defects in Solids **157**, 799 (2002)
13. G. Kalpana, B. Palanivel, I.B. Shameem Banu, Phys. Rev. B **56**, 3532 (1997)

14. G. Kalpana, B. Palanivel, K. Venkatasubramaniam, M. Rajagopalan, Bull. Mater. Sci. **20**, 461 (1997)
15. M. Sieskind, M. Ayadi, G. Zachmann, Phys. Stat. Sol. **136**, 489 (1986)
16. K.R. Balasubramanian, T.M. Haridasan, J. Phys. Chem. Solids **42**, 667 (1981)
17. K.R. Balasubramanian, T.M. Haridasan, N. Krishnamurthy, Chem. Phys. Lett. **67**, 530 (1979)
18. R. Mittal, S.L. Chaplot, A. Sen, S.N. Achary, A.K. Tyagi, Appl. Phys. A **74**, 1109 (2002)
19. F. Decremps, M. Fischer, A. Polian, J.P. Itié, Eur. Phys. J. B **5**, 7 (1998)
20. F. Decremps, M. Fischer, A. Polian, J.P. Itié, Phys. Rev. B **59**, 4011 (1999)
21. V.R. Saunders, R. Dovesi, C. Roetti, R. Orlando, C.M. Zicovich-Wilson, N.M. Harrison, K. Doll, B. Civalleri, I.J. Bush, P. D'Arco, M. Llunell, *CRYSTAL03 User's Manual, 2003*, Università di Torino, Torino
22. Y.R. Shen, T. Gregorian, W.B. Holzapel, High Pressure Res. **7**, 73 (1991)
23. Y.R. Shen, U. Englisch, L. Chudinovskikh, F. Porsch, R. Haberkorn, H.P. Beck, W.B. Holzapfel, J. Phys.: Condens. Matt. **6**, 3197 (1993)
24. M. Sonada, M. Takano, J. Miyahara, H. Kato, Radiology **148**, 833 (1991)
25. K. Takahashi, J. Miyahara, Y. Shibahara, J. Electrochem. Soc. **132**, 1492 (1985)
26. P.A.M. Dirac, Proc. Camb. Phil. Soc. **26**, 376 (1939)
27. J.P. Perdew, Y. Wang, Phys. Rev. B **33**, 8800 (1986)
28. J.P. Perdew, Y. Wang, Phys. Rev. B **40**, 3399 (1989)
29. J.P. Perdew, Y. Wang, Phys. Rev. B **45**, 13244 (1992)
30. J.P. Perdew, *Electronic Structure of Solids* (Akademie Verlag, Berlin, 1991)
31. A.D. Becke, J. Chem. Phys. **98**, 5648 (1993)
32. C. Lee, W. Yang, R.G. Parr, Phys. Rev. B **37**, 785 (1988)
33. N.M. Harrison, V.R. Saunders, J. Phys.: Condens. Matter **4**, 3873 (1992)
34. M. Catti, R. Dovesi, A. Pavese, R. Saunders, J. Phys.: Condens. Matter **3**, 4151 (1991)
35. P.J. Hay, W.R. Wadt, J. Chem. Phys. **82**, 270 (1985)
36. P.J. Hay, W.R. Wadt, J. Chem. Phys. **82**, 284 (1985)
37. P.J. Hay, W.R. Wadt, J. Chem. Phys. **82**, 299 (1985)
38. *LoptCG (Shell procedure for numerical gradient optimisations)* written and developed by C.M. Zicovich-Wilson, Universidad Autonoma del Estado de Morelos, Mexico, 1998
39. K. Doll, N.M. Harrison, V.R. Saunders, Int. J. Quantum Chem. **82**, 1 (2001)
40. K. Doll, Comp. Phys. Comm. **137**, 74 (2001)
41. R. Orlando, V.R. Saunders, R. Dovesi, unpublished
42. H.B. Schlegel, J. Comp. Chem. **3**, 214 (1982)
43. B. Civalleri, Ph. D'Arco, R. Orlando, V.R. Saunders, R. Dovesi, Chem. Phys. Lett. **348**, 131 (2001)
44. S.H. Vosko, L. Wilk, M. Nusair, Can. J. Phys. **58**, 1200 (1980)
45. F. Pascale, C.M. Zicovich-Wilson, F. Lopez Gejo, B. Civalleri, R. Orlando, R. Dovesi, J. Comp. Chem. **25**, 888 (2004)
46. M. Born, K. Huang *Dynamical Theory of Crystal Lattices* (Oxford Univ. Press, Oxford, 1954)
47. P. Umari, A. Pasquarello, A.D. Corso, Phys. Rev. B **63**, 094305 (2001)
48. M. Sauvage, Acta Cristallogr. Sect. B: Struct. Crystallogr. Cryst. Chem. **30**, 2786 (1974)
49. M. Mérawa, P. Labéguerie, P. Ugliengo, K. Doll, R. Dovesi, Chem. Phys. Lett. **387**, 453 (2004)
50. *Janaf Thermodynamical Tables*, J. Phys. Chem. Ref. Data Suppl. **1**, 14 (1985)
51. P. Baranek, A. Lichanot, R. Orlando, R. Dovesi, Chem. Phys. Lett. **340**, 362 (2001)
52. J.F. Scott, J. Chem. Phys. **49**, 2766 (1968)
53. H.L. Bhat, M.R. Srinivasan, S.R. Girisho, A.H. Rama Rao, P.S. Narayanan, Indian, J. Pure Appl. Phys. **15**, 74 (1977)
54. D. Nicollin, H. Bill, J. Phys. C: Solid State Phys. **11**, 4803 (1978)
55. P. Ugliengo, `http://www.theochem.unito.it/moldraw/moldraw.html` (2003), MOLDRAW
56. M. Mérawa, M. Llunell, R. Orlando, M. Gelize-Duvignau, R. Dovesi, Chem. Phys. Lett. **368**, 7 (2003)
57. M. Mérawa, B. Civalleri, P. Ugliengo, Y. Noel, A. Lichanot, J. Chem. Phys. **119**, 1045 (2003)
58. X. Xu, W.A. Goddard III, PNAS **101**, 2673 (2004)
59. T. Yanai, D.P. Tew, N.C. Handy, Chem. Phys. Lett. **393**, 51 (2004)